WEP Warwick Evans Publishing

International Journal of Mechanical and Electrical Engineering

ISSN: 3005-9615 (Print), ISSN: 3005-7132 (Online) | Volume 8, Number 4, Year 2026
DOI: https://doi.org/10.62051/ijmee.v8n4.02
Journal homepage: https://wepub.org/index.php/IJMEE/index

Control Method for Lateral Vibration of High-Speed Trains under Crosswind

Chuanhui Zhao *, Xiangfeng Kong

College of Locomotive and Rolling Stock Engineering, Nanjing Vocational Institute of Railway Technology, Nanjing, Jiangsu, China

* Corresponding Author: Chuanhui Zhao

ABSTRACT

This paper addresses the issue of lateral vibration of high - speed train car bodies caused by random track irregularity excitation and random wind excitation. It proposes an active control method based on the SABO - LQR algorithm and the secondary suspension system to enhance the running stability and safety of high - speed trains by suppressing the lateral vibration of the car body. First, a dynamic model of the cross - wind - vehicle - track system is established, taking into account both random track irregularity excitation and random wind excitation. Second, considering the difficulty in selecting the weight matrices Q and R during the design of the LQR controller, the SABO algorithm is used for iterative optimization to obtain the optimal weight matrices and the controller. Finally, the effectiveness of the proposed method is further verified through simulation. The results show that the proposed active control method based on the SABO - LQR algorithm and the secondary suspension system has the potential to effectively suppress the lateral vibration of the train car body. Compared with the passive suspension method and the LQR control method, this method can reduce the amplitude of the car body's lateral vibration by 67.13% and 50.30% respectively, thus improving the riding comfort and the running stability of high - speed trains.

KEYWORDS

Crosswinds; Active Suspension; Lateral Vibration; SABO; LQR Control.

1. INTRODUCTION

In recent years, China's railway network has been continuously expanding, and trains have been developing towards lightweight and high - speed. The impact of cross - winds on the operation of high-speed trains has become increasingly prominent. Lines such as the Lanzhou-Xinjiang Railway, the Southern Xinjiang Railway, and coastal railways are often affected by strong cross - winds. Under cross - wind conditions, the aerodynamic load of trains increases significantly, and the lateral vibration of the train body intensifies, which directly threatens the safety of train operation and the riding comfort [1]. Therefore, conducting research on the active control of the lateral vibration of high - speed trains in cross - wind environments is of great practical significance for ensuring train safety and improving passenger comfort.

With the development of actuator and control technologies, active suspension has become an important means to improve the running safety of trains under cross - winds. Most of the existing research focuses on two aspects: new - type actuators and control strategies. Some studies adjust the wheel - rail force and the attitude of the car body by means of electromagnetic suction [2] and giant magnetostrictive actuators [3] to suppress vertical or lateral vibration. The other part focuses on control algorithms, such as improved sky - hook control [4], fuzzy control [5], sliding mode control

[6], neural network and adaptive control [7], which have all achieved vibration reduction and efficiency improvement to a certain extent. However, most of the existing research results do not simultaneously consider the problem of suppressing the lateral vibration of trains under the combined action of cross - winds and track excitations.

In this paper, we introduce the subtraction average based optimizer (SABO) and linear quadratic regulator (LQR) into the active suspension system to regulate the lateral vibration acceleration of the vehicle body and enhance the operational stability. The remainder of this paper is organized as follows. In Section 2, a crosswind-vehicle-track coupled dynamics model is established, in which the random track irregularity and unsteady aerodynamic loads are considered. Then, the control strategy and method analysis are introduced in Section 3. In Section 4, the numerical simulations and results discussion are presented. Finally, some conclusions are drawn in Section 5.

2. CROSSWIND-VEHICLE TRACK COUPLED DYNAMICS MODEL

2.1. 1/4 High-Speed Train Lateral Vibration Model

This paper mainly focuses on the lateral vibration acceleration of the high - speed train car body's center of mass under the action of cross - winds and its control. To simplify the complexity of the dynamic model of the train's active suspension and the design of the LQR controller, a 1/4 lateral active suspension model of the high - speed train is established in combination with Reference [8], as shown in Figure 1.

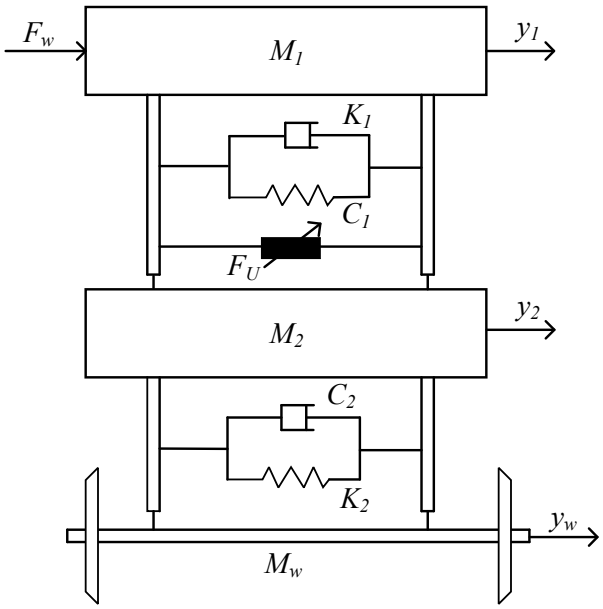

Figure 1. 1/4 Model of high-speed train

Based on Figure 1 and Newton's laws of motion, establish the motion differential equation of this model.

$$\begin{cases} M_1\ddot{x}_1 + C_1(\dot{x}_1 - \dot{x}_2) + K_1(x_1 - x_2) - F_U - F_w = 0 \\ M_2\ddot{x}_2 + C_1(\dot{x}_2 - \dot{x}_1) + K_1(x_2 - x_1) + K_2(x_2 - g) + C_2(\dot{x}_2 - \dot{g}) + F_U = 0 \end{cases}. \quad (1)$$

In the formula, M_1 and M_2 are the mass of the car body and the mass of the bogie respectively, g is the excitation of track horizontal irregularity, F_w is the cross - wind excitation, and F_U is the active

control force generated by the active actuator in the secondary suspension system. The meanings and parameters represented by each letter are listed in Table 1.

Table 1. High-speed train parameter

parameter	numerical value
Vehicle body mass M_1[kg]	400 00
Quality of the steering frame structure M_2[kg]	320 0
Spring stiffness of the second suspension system K_1[N·m^{-1}]	800 000
Damping coefficient of the second suspension system C_1[N·s·m^{-1}]	120 000
Spring stiffness of the suspension system K_2[N·m^{-1}]	208 000 0
Damping coefficient of the suspension system C_2[N·s·m^{-1}]	100 000

Among them, the system state variables is $\boldsymbol{X}=[x_2 \quad x_1 \quad \dot{x}_2 \quad \dot{x}_1]^{\mathrm{T}}$,The active suspension control outputs take into account the vehicle body acceleration, the suspension movement stroke and the displacement of the steering frame,then $\boldsymbol{Y}=[\ddot{x}_1 \quad x_1-x_2 \quad \dot{x}_2]^{\mathrm{T}}$,The controlled variable is $\boldsymbol{U}=[F_U]$,The interference level is $\boldsymbol{G}=[g \quad \dot{g} \quad F_W]^{\mathrm{T}}$.

Then the state space equation of the system can be written as:

$$\begin{cases} \dot{X}=AX+BU+G\omega(t) \\ Y=Cx+DU \end{cases}. \tag{2}$$

Where,

$$\boldsymbol{A}=\begin{bmatrix} 0 & 0 & 1 & 0 \\ 0 & 0 & 0 & 1 \\ \dfrac{-k_1}{m_1} & \dfrac{k_1}{m_1} & \dfrac{-c_1}{m_1} & \dfrac{c_1}{m_1} \\ \dfrac{k_1}{m_2} & \dfrac{-(k_1+k_2)}{m_2} & \dfrac{c_1}{m_2} & \dfrac{-(c_1+c_2)}{m_2} \end{bmatrix}, \quad \boldsymbol{B}=\begin{bmatrix} 0 \\ 0 \\ \dfrac{1}{m_1} \\ \dfrac{-1}{m_2} \end{bmatrix},$$

$$\boldsymbol{C}=\begin{bmatrix} \dfrac{-k_1}{m_1} & \dfrac{k_1}{m_1} & \dfrac{-c_1}{m_1} & \dfrac{c_1}{m_1} \\ 1 & -1 & 0 & 0 \\ 0 & 0 & 0 & 1 \end{bmatrix}, \quad \boldsymbol{D}=\begin{bmatrix} \dfrac{1}{m_1} \\ 0 \\ 0 \end{bmatrix}, \quad \boldsymbol{G}=\begin{bmatrix} 0 & 0 & 0 \\ 0 & 0 & 0 \\ 0 & 0 & \dfrac{1}{m_1} \\ \dfrac{k_2}{m_2} & \dfrac{k_2}{m_2} & 0 \end{bmatrix}.$$

2.2. Track Irregularity Excitation

In the research on the safety of high-speed train operation, due to the obvious randomness of the track conditions in the actual lines, in order to better simulate the random characteristics of track irregularities during high-speed train operation, the track irregularity excitation is generally regarded as the input of the system. The commonly used power spectra of track irregularities include the German track spectrum, the American track spectrum, and the track irregularity spectrum of China's high-speed railway ballastless track proposed by the China National Railway Administration in 2014. This paper uses the time-domain irregularity samples converted from the track irregularity spectrum of China's high-speed railway ballastless track as the track irregularity excitation.

The expression of the track irregularity spectrum of China's high-speed railway ballastless track is [9]:

$$S(\phi) = \frac{A}{\phi^n}. \tag{3}$$

where, A and n represent the coefficients of the fitting formula; $S(\phi)$ represents the power spectral density function, $mm^2/(1/m)$; ϕrepresents the spatial frequency of the track random irregularity, (1/m).

The numerical simulation was carried out using the inverse Fourier transform method, thereby providing the orbital input excitation for the study of linear and nonlinear system vibrations. The process and steps [10] are as follows:

(1) Suppose the running speed of the high-speed train is v, and the maximum and minimum wavelengths of track irregularities are λ_{max} and λ_{min} respectively. Then:

$$f_{min} = \frac{v}{\lambda_{max}}. \tag{4}$$

$$f_{max} = \frac{v}{\lambda_{min}}. \tag{5}$$

In Equations (2) and (3), $f_{\max}$ and $f_{\min}$ represent the upper and lower cutoff frequencies of the simulation frequency band. According to the sampling theorem, the sampling time interval in the time domain is set as Δt:

$$\Delta t \le \frac{f_{max}}{2}. \tag{6}$$

Assuming the total simulation time is T, then the number of time-domain sampling points is:

$$N = \frac{T}{\Delta t}. \tag{7}$$

Among them, N is an integer power of 2, and the frequency sampling time and the number of sampling points within the effective frequency band are:

$$\Delta f = \frac{1}{N \times \Delta t}. \tag{8}$$

$$N_f = \frac{f_{max} - f_{min}}{\Delta f}. \tag{9}$$

Due to the characteristic of the periodic method, the sampling point values within the sampling segment from($N/2$-N_f)~($N/2$+N_f) are assumed to be 0. Then, in the sampling segment from 1 to $N/2$, the sampling point values of the orbital spectrum $S_a(f)$=(f=$k\cdot\Delta f$,k=0,1,2,…$N/2$).

(2)By using the periodic diagram method, it can be obtained that:

$$\left|X(k)\right| = \left|DEF\left[x(n)\right]\right| = \sqrt{N^2 \cdot S_a(k)} = \sqrt{S_a(f = k \cdot \Delta f)\Delta f}\ (k = 0,1,...N-1) \tag{10}$$

where, $|X(k)|$represents the simulated value of the spectrum $X(k)$ of the random sequence $x(n)$. In an independent phase sequence, when ψ_n satisfies the condition $|\psi_n|$=1, then:

$$\psi_n = \cos\Phi_n + i\sin\Phi_n = \exp(i\cdot\Phi_n)\,. \tag{11}$$

$$X(k) = \psi_n \cdot N\sqrt{S_a(f = k\cdot\Delta f)}\,. \tag{12}$$

By applying Fourier transformation to Equations (9) and (10), we can obtain:

$$x(n) = \mathrm{Re}(\frac{1}{N}\sum_{k=0}^{N-1} X(k)\exp[\frac{i2\pi nt}{N}])\,. \tag{13}$$

Based on Equations (3) - (13), the time-domain simulation diagram of the unevenness of the ballastless track in our country and the numerical fitting comparison diagram after Fourier transformation can be obtained, which are respectively shown in Figure 2 and Figure 3.

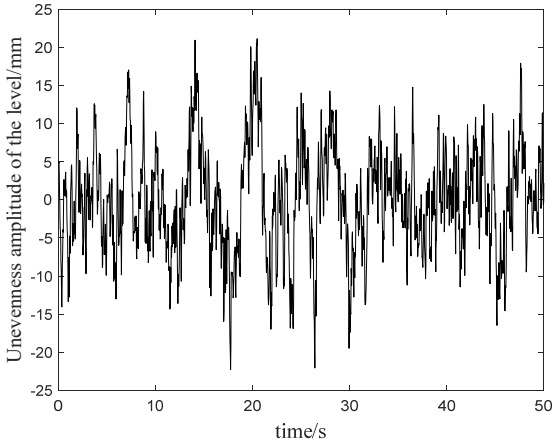

Figure 2. Numerical simulation of uneven track spectra

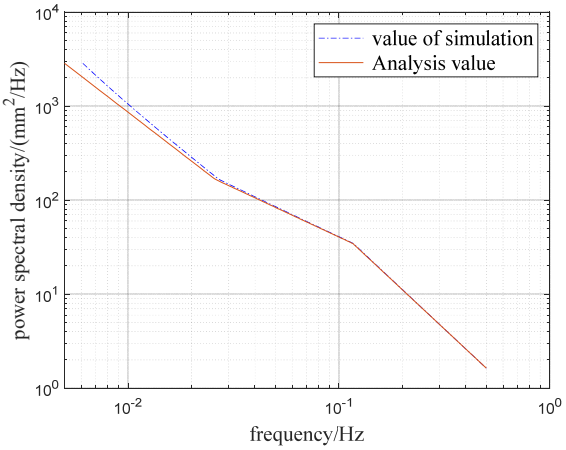

Figure 3. Comparison of simulated and analytical values of the unevenness spectrum of the track

2.3. Unsteady Aerodynamic Loads

TIn the side wind model of high-speed trains, the instantaneous wind speed consists of the mean wind and the fluctuating wind. The wind speed value ω at any point can be expressed as[11]:

$$\omega = \bar{\omega} + \omega'\,. \tag{14}$$

The power spectral density can describe the characteristics of random fluctuating wind speed. Cooper derived the power spectral density function of pulsating wind [12] as follows:

$$\frac{NS_\omega}{\sigma_\omega^2}=\left[\frac{4\left(NL'/\overline{u}\right)}{1+70.8((NL'/\overline{u})^2)^{5/6}}\right]\times\left[C_u{}^2+\left(1-C_u{}^2\right)\frac{0.5+94.44(NL'/\overline{u})^2}{1+70.8(NL'/\overline{u})^2}\right]. \tag{15}$$

$$C_u=v\cos\alpha/\overline{u}+\overline{\omega}/\overline{u}\,. \tag{16}$$

$$L'=L_w^x\left[C_u^2+4(L_w^y/L_w^x)^2\left(1-C_u^2\right)\right]^{0.5}. \tag{17}$$

where, S_ω, σ_ω and $NS_\omega/\sigma_\omega^2$ respectively represent the power spectral density, standard deviation and dimensionless power spectral density of the fluctuating wind speed, $\sigma_\omega=\overline{w}L_Z$, where L_Z represents the turbulence intensity, N represents the frequency, and L_W^x , L_W^y respectively represent the longitudinal and lateral turbulence integral scales. u repre sents the average synthesized wind speed, and its expression is:

$$\overline{u}=\sqrt{v^2+\overline{\mathrm{w}}^2+2v\overline{\mathrm{w}}\cos\alpha}\,. \tag{18}$$

The intensity of turbulence is related to the surface roughness length and the height above the ground. The calculation is as shown in Equation (19):

$$L_z=\frac{1}{\ln(M/M_0)}\left(1-5\times10^{-5}\left(\log(\frac{M_0}{0.05}\right)+2)^7\right). \tag{19}$$

In the formula, M and M_0 represent the ground height and roughness length respectively.

The turbulent integral scale can be expressed as:

$$L_w^x=50\times\frac{z^{0.35}}{z_0^{0.063}}\,. \tag{20}$$

$$L_w^y=0.42L_w^x. \tag{21}$$

The power spectral density value can be obtained through calculation. The pulsating wind speed v can be obtained through the harmonic superposition method, and the calculation formula is:

$$\omega'=\sum_{\mathrm{i}}\left[2S_\omega\left(N_i\right)\Delta N_i\right]^{0.5}\sin(2\pi N_iT+2\pi R_i)\,. \tag{22}$$

where, T represents time, ΔN_i denotes the step size of frequency, and R_i is a random number ranging from 0 to 1.

The unsteady aerodynamic load F is composed of the average wind force $\overline{F}$ and the pulsating wind force F'. Then, we have:

$$F=\overline{F}+F'=0.5\rho A(\overline{u}+u')^2\cdot C_F\left(\beta\right). \tag{23}$$

where, the average wind force acting on the center of mass of the high-speed train, denoted as $\overline{F}$, is shown in Equation (17).

$$\overline{F}=0.5\rho AV^2C_F\left(\beta\right). \tag{24}$$

where, ρ represents the air density, A is the equivalent area of the windward side of the high-speed train, and $C_F(\beta)$ is the side force dynamic coefficient.

In an on-wind environment, when $\alpha = 90°$, there is:

$$F' = \rho A \overline{C}_F \overline{\omega} \left(1 + \frac{0.5 \overline{C'}_F \cot \overline{\beta}}{\overline{C}_F} \right) \times \int_0^{\infty} h_F(\tau) \omega'(t-\tau) d\tau \quad . \tag{25}$$

where, $\overline{C'}_F$ represents the value of the derivative of $C_F(\beta)$ at β, where, β is the sideslip angle. h_F is the aerodynamic weight function, and its value is:

$$h_F(\tau) = \left(2\pi \overline{n}' \overline{u} / L' \right)^2 \tau \exp(-2\pi n' \overline{u} / L') \tau \, . \tag{26}$$

where, $\overline{n}'$ represents the dimensionless frequency.

For calculating the aerodynamic moment, it is only necessary to replace the aerodynamic coefficient with the aerodynamic moment coefficient, and add the reference height to the aerodynamic calculation formula. The method for calculating the aerodynamic load coefficient refers to reference [13].

According to the above formula, the lateral aerodynamic load of the high-speed train is calculated as the lateral wind excitation of the train model. The time history curve of the aerodynamic load when the average wind speed is 20 m/s and the train speed is 200 km/h is shown in Figure 3.

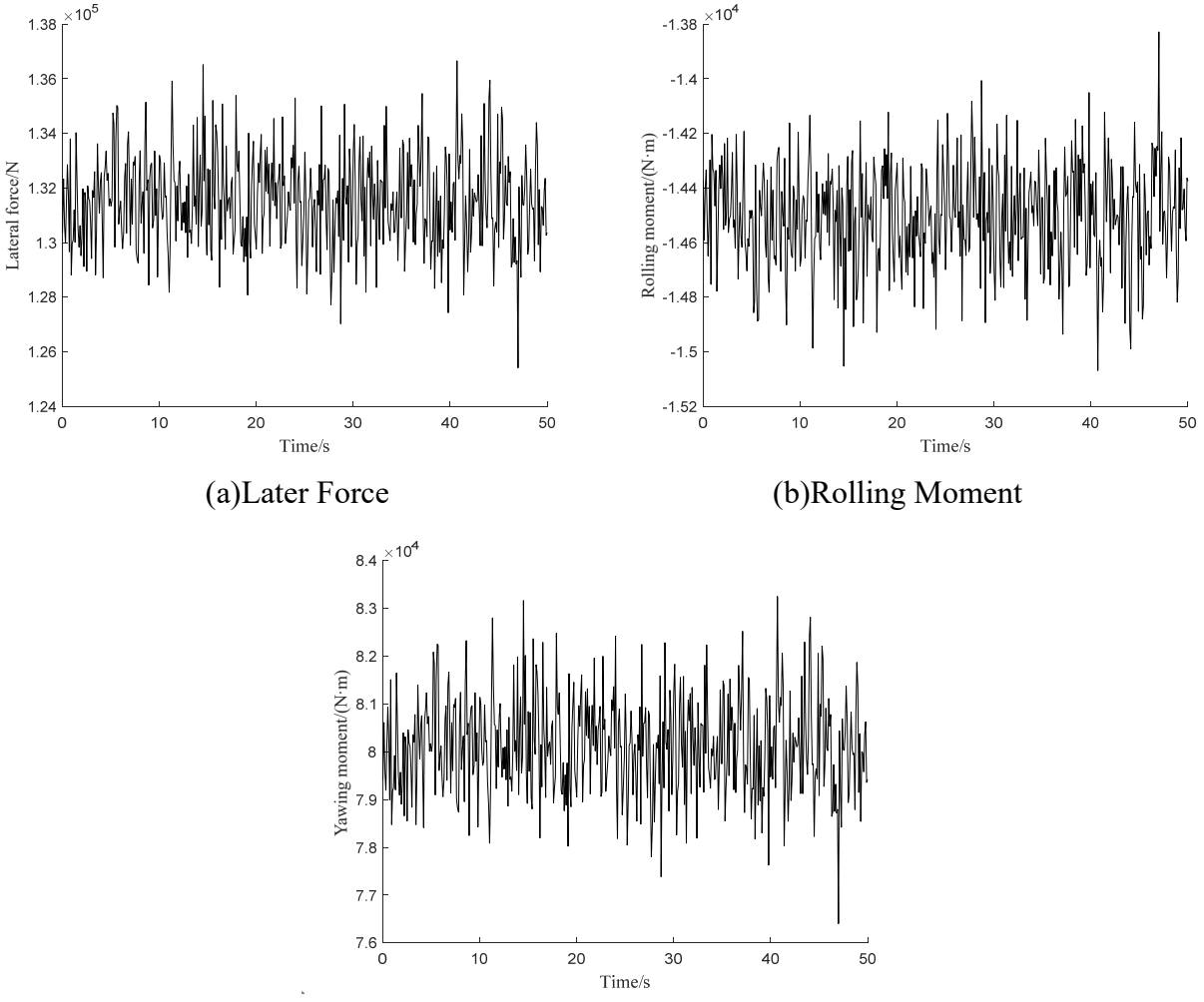

(a)Later Force (b)Rolling Moment

(c)Yawing Moment

Figure 4. Aerodynamic Loads

3. LQR CONTROLLER AND ITS ALGORITHM DESIGN

3.1. LQR Controller

The active suspension of the vehicle is controlled using LQR. The control targets are the lateral vibration acceleration of the vehicle body, the dynamic travel of the suspension, and the displacement of the bogie. Then, the performance index function can be defined as

$$J = \lim_{T\to\infty}\frac{1}{T}\int_0^T\left[\rho_1\ddot{x}_1^2 + \rho_2\left(x_1 - x_2\right)^2 + \rho_3 x_2^2 + rF_U^2\right]\mathrm{d}t . \tag{27}$$

Among them, ρ_1, ρ_2, and ρ_3 are the weighting coefficients for the three controlled quantities in the control target, and r is the weighting coefficient for the active control force. $\boldsymbol{\rho} = \mathrm{diag}\left(\rho_1, \rho_2, \rho_3\right)$ respectively reflect the degree of importance given to each controlled quantity and the active control force provided by the system. By taking the weighting matrix, the performance functional represented by Equation (27) can be written as

$$\begin{aligned} J &= \lim_{T\to\infty}\frac{1}{T}\int_0^T (Y^T\rho Y + F_U^T r F_U)dt = \lim_{T\to\infty}\frac{1}{T}\int_0^T\left[(CX + DF_U)^T\rho\left(CX + DF_U\right) + F_U^T r F_U\right]dt \\ &= \lim_{T\to\infty}\frac{1}{T}\int_0^T [X^T C^T\rho CX + 2X^T C^T\rho DF_U + F_U^T\left(D^T\rho D + r\right)F_U]dt \end{aligned} . \tag{28}$$

If $Q = C^T\rho C$, $N = C^T\rho D$, $R = D^T\rho D + r$, then the feedback gain matrix is

$$H = R^{-1}B^T P . \tag{29}$$

Matrix ***P*** can be obtained by solving the Riccati equation, that is

$$A^T P + PA - PBR^{-1}B^T P + Q = 0 . \tag{30}$$

Then the control force of the actuator is expressed as

$$F_U\left(t\right) = -HX \tag{31}$$

3.2. SABO Algorithm Optimizes the LQR Controller

Although the LQR controller in analytical form has fast control calculation speed, is easy to implement in engineering and can ensure the real-time performance of control, the weight matrix coefficients need to be calculated manually through trial and error, which is time-consuming and labor-intensive. To improve the effect of the LQR controller, it is necessary to select reasonable coefficients.

The Subtraction Average Based Optimizer (SABO) algorithm is an innovative meta-heuristic algorithm. Its core lies in using mathematical principles, especially concepts such as average values and position differences, to guide the search strategy in the optimization process. It has the characteristics of strong optimization ability and fast convergence speed.

SABO is based on a special operation '-v' , called the'-v' of search agent B and search agent A, expressed as formula (32).

$$A -_v B = \mathrm{sign}(F(A) - F(B))\ (A - \vec{v} * B) . \tag{32}$$

where, $\vec{v}$ represents an *m*-dimensional vector, where the components are random numbers generated from the set [1, 2], $F(A)$ and $F(B)$ represent the objective function values corresponding to search agent *A* and search agent *B* respectively, sign represents the function of signum.

The displacement of search agent X_i in the search space is calculated by the arithmetic average of the '-*v*' operation between search agent X_j and X_i (i, j=1, 2, …, *N*), and the calculation formula is as shown in Equation (33).

$$X_i^{new} = X_i + \vec{r}_i * \frac{1}{N}\sum_{j=1}^{N}(X_i -_v X_j) . \tag{33}$$

where, X_i^{new} represents the updated position of the *i*-th search agent X_i (*i*=1, 2, …,*N*), *N* represents the total number of particles, $\vec{r}_i$ represents an m-dimensional vector.

The new position X_i^{new} after update can improve the value of the objective function, and thus can be regarded as the new position for the corresponding agent. The particle position replacement formula is shown in Equation (34).

$$X_i = \begin{Bmatrix} X_i^{new}, & F_i^{new} < F_i \\ X_i \quad , & else \end{Bmatrix} . \tag{34}$$

where, F_i , F_i^{new} represents the objective function value of search agent X_i and X_i^{new} .

SABO can be used to optimize the coefficients of LQR controllers, improving the control effect.

Chaotic mapping has significant advantages in initializing the population, helping to evenly distribute individuals within the search space and increasing population diversity; moreover, chaotic mapping can quickly discover multiple potential optimal solutions. The Logistic chaotic mapping, as one of the simplest chaotic systems, is represented by a simple iterative equation and is easy to understand and implement. It only requires two variables (current state and control parameters) to achieve.

$$x_{i+1} = 4x_i(1 - x_i) . \tag{35}$$

Where, $0 \le x_i \le 1$， i=1,2,… .

The optimization steps are as follows:

Step 1: Initialization, Use a chaotic mapping to initialize the population, ensuring diversity among the particles and accelerating the convergence of the algorithm.

Step 2: Calculate the fitness values of all particles based on the fitness function and the Simulink model.

Step 3: At the beginning of the iteration, search and update the positions of the examples according to the position formula.

Step 4: Save the optimal individual.

Step 5: Determine whether the termination conditions are met. If they are, terminate the program and output the optimal value; if not, return to step 2 to continue the iteration.

4. SIMULATION VERIFICATION

To verify the effectiveness of the proposed SABO optimized LQR controller in suppressing the lateral vibration of the train, the Chinese ballastless track spectrum and aerodynamic load were used as the excitation input for the train model, and a performance comparison test of LQR control was conducted.

The root mean square (RMS) of the lateral displacement acceleration of the vehicle body was calculated to evaluate its driving stability.

4.1. Simulation Model Setup

Figure 5 shows the Simulink model of the LQR controller for the high-speed train. The simulation parameters are: wind speed of 20 m/s and train speed of 300 km/h.

The dynamics simulation of the active suspension was completed using Matlab/Simulink. The sampling period T was set to 0.01 seconds, and the simulation time was set from 0 to 50 seconds. The lateral acceleration of the system, the suspension displacement, and the lateral acceleration of the frame were selected as the real-time observed values of the model.

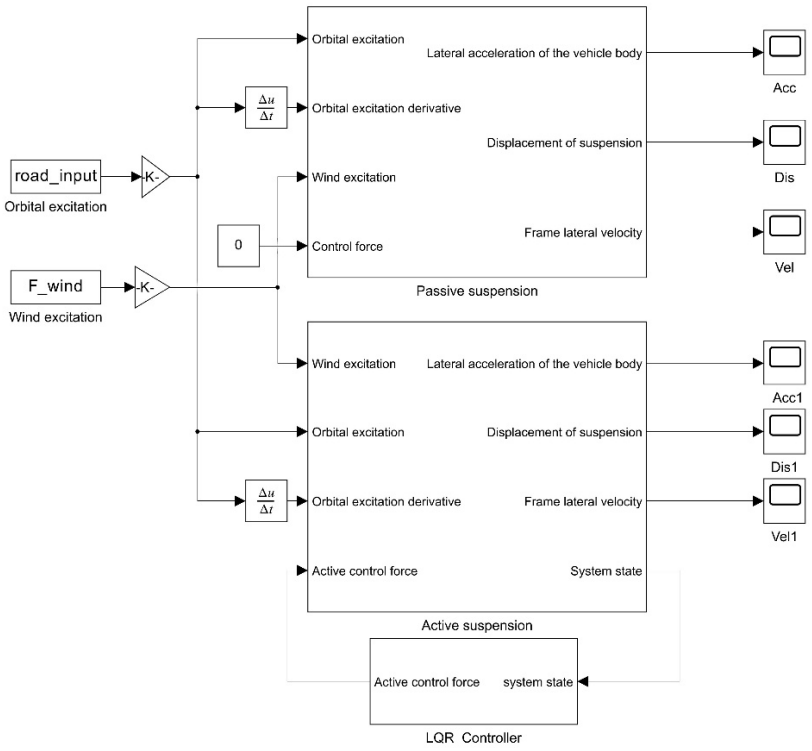

Figure 5. Simulation Model Diagram

4.2. Simulation Results Comparison

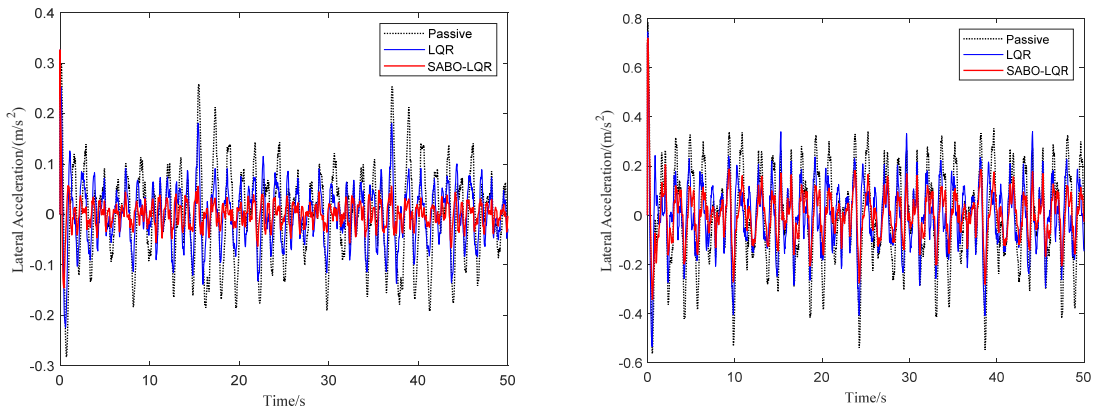

(a) 200km/h (b) 300km/h

Figure 6. Comparison Chart of Lateral Acceleration

The active control simulation was carried out using Matlab. The controller was optimized through the SABO algorithm, enabling the active suspension system to achieve better control performance under crosswind conditions. The simulation results are shown in Figures 6 and Figures 7, and the control effect is listed in Table 2.

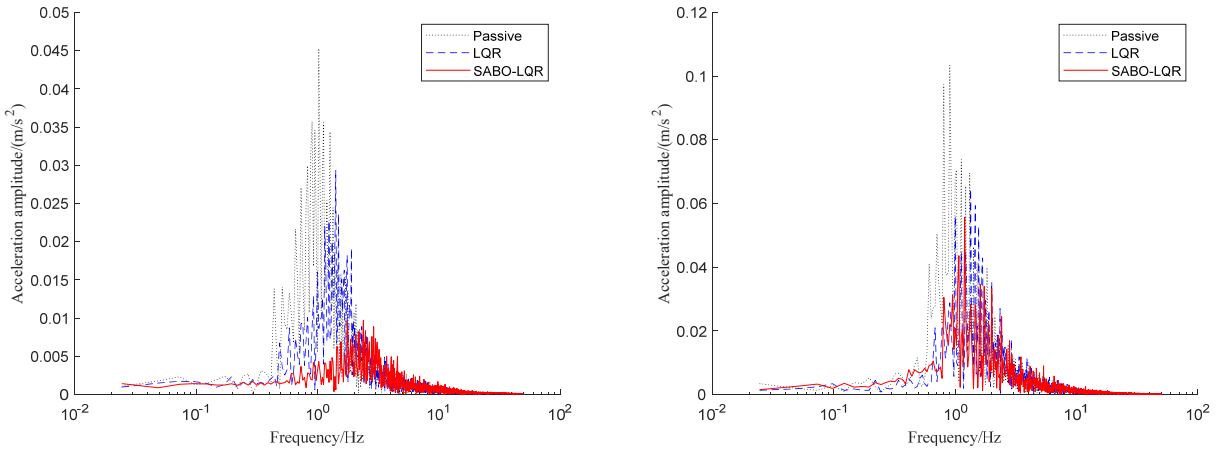

(a) 200km/h (b) 300km/h

Figure 7. Frequency Domain Diagram of Lateral Acceleration

Table 2. Comparison of root mean square values of system acceleration

Speed / Control Method	RMS	
	200[km/h]	300[km/h]
PassiveControl	0.090309	0.19174
LQR Control	0.059731	0.13634
SABO -LQR Control	0.029685	0.10141

From the data in Figure 6 and Table 2, it is clearly evident that compared with passive suspension control, the LQR controller can reduce the lateral vibration acceleration of the train throughout the simulation period, and the maximum reduction in the RMS value of the lateral vibration acceleration of the train body reaches 33.86%; especially after optimizing the LQR controller through the SABO algorithm, the effect of suppressing the lateral vibration of the train body is more significant. Specifically, when compared with passive suspension and LQR control methods respectively, the maximum reduction in the RMS value of the lateral vibration acceleration of the train body by the SABO-LQR control method reaches 67.13% and 50.30% respectively.

As can be clearly seen from Figure 7, compared with the passive suspension control, during the entire simulation period, the frequency domain values of the lateral vibration acceleration of the vehicle body under the LQR and SABO-LQR control methods both decreased. Thus, it can be concluded that the LQR controller has a more obvious effect in controlling the lateral vibration of the train in cross-wind conditions. Especially, the frequency domain value of the lateral vibration acceleration of the vehicle body under the SABO-LQR control method is the smallest, and its control effect is better. The results show that the SABO-LQR active control method can effectively improve the lateral vibration of high-speed trains in cross-wind conditions, significantly enhancing the safety of high-speed train operation in cross-wind conditions, and verifying the rationality and effectiveness of the SABO-LQR active control method.

5. SUMMARY

5.1. Summar

This paper reports an efficient active suspension system that adopts the SABO-LQR control method to suppress the lateral vibration of high-speed trains under strong crosswind conditions and enhance operational safety. A side wind - vehicle - track coupled dynamic mechanical model was established, and the performance of the proposed active suspension system was verified. The results show that the method proposed in this paper can significantly reduce the amplitude of the train's lateral vibration, and has good dynamic response performance, robustness and superiority. It greatly improves the ride comfort and operational stability of high-speed train vehicles in the lateral direction, and also enhances the operational safety of high-speed trains in complex environments. The research results of this paper have strong guiding significance and reference value for the control and safety management of train lateral vibration.

CONFLICTS OF INTEREST

The authors declare that they have no conflict of interest.

ACKNOWLEDGMENTS

The author(s) disclosed receipt of the following financial support for the research, authorship, and/or publication of this article: This work was supported by the School-level Excellent Innovation and Technology Research Team of Nanjing Vocational Institute of Railway Technology [Grant number CXTD2025002].

REFERENCES

[1] Yang Weichao, Deng E, Zhu Zhihui, et al. Sudden Variation Effect of Aerodynamic Loads and Safety Analysis of Running Trains When Entering Tunnel Under Crosswind [J].Applied Sciences,2020,Vol.10(4): 1445.

[2] Zhang Heng, Ling Liang, Chang Chao, et al. Research on wind induced safety active control of high-speed trains based on linear track eddy current brakes [J]. Journal of Mechanical Engineering, 2022, 58 (08)：195-203.

[3] Li DC, Meng JJ, Bai H, et al. Active control strategy for the running attitude of high-speed train under strong crosswind condition. Vehicle System Dynamics, 2018, Vol. 56(7): 1028-1050.

[4] Zhou Chuanghui, Wen guilin. Hydraulic-electrical energy regenerative semi-active hydro-pneumatic suspension system based on a modified skyhook damping control algorithm[J]. Journal of Vibration and Shock, 2018, 37(14): 168-174+207.

[5] Zhang Ruidong, Meng Jianjun, Li Decang. Study on Fuzzy Adaptive PID Control of High-speed Train Semi-active Suspension System[J]. 2023, 43(02): 1-7.

[6] Wang Xinyue; Huang Deqing; Qin Na; et al. Modeling and Second-Order Sliding Mode Control for Lateral Vibration of High-Speed Train With MR Dampers[J]. IEEE TRANSACTIONS ON INTELLIGENT TRANSPORTATION SYSTEMS, 2022, Vol. 23(8): 10299-10308.

[7] J. W. Yang, J. Li, and Y. P. Du, “Adaptive fuzzy control of lateral semiactive suspension for high-speed railway vehicle,” in Proc. Int. Conf. Intell. Comput., Kunming, China, 2006, pp. 1104-1115.

[8] CHEN Chunjun. Active and semi-active control of high-speed trains [M]. Chengdu：Southwest Jiaotong University Press, 2010.

[9] Li Guangjun, Mao Xiangwen, Ding Jiahui. Design of a numerical simulation experimental system for track irregularity input[J]. Experimental Technology and Management, 2019, 36 (05): 123-125.

[10] Niu Liubin, LIU Jinchao, Qu Jianjun, et al. Correlation Model of Track Irregularity and Lateral Acceleration of Car Body Based on State Space Method [J]. Journal of the Chinese Journal of Railways, 2020, 42(08): 123-129.

[11] Wang Xiwen, Qi Wenzhe, Li Decang, et al. Dynamic safety characteristics of high-speed trains under random wind loads[J]. Science and Technology and Engineering, 2023, 23 (23): 10085-10090.

[12] Yu Mengge, Zhang Qian, Liu Jiali, et al. Study on the Operational Safety Evaluation of The High-speed Train Exposed to Stochastic Winds[J]. Journal of Mechanical Engineering, 2018, 54(4); 245-254.

[13] SHENG Xugao, Yu Mengge, Li Tian, et al. Multi-objective Wind-resistant optimization Design of high-speed Train Dynamic Parameters [J]. Journal of Machine Design, 2023, 40(01): 1-7.

[14] Yang, J., Li, J., Du, Y. (2006). Adaptive Fuzzy Control of Lateral Semi-active Suspension for High-Speed Railway Vehicle. In: Huang, DS., Li, K., Irwin, G.W. (eds) Computational Intelligence. ICIC 2006. Lecture Notes in Computer Science, vol 4114. Springer, Berlin, Heidelberg.